

# Targeting Tumor Angiogenesis: Comparison of Peptide and Polymer-Peptide Conjugates

Bruce R. Line, MD<sup>1-3</sup>; Amitava Mitra, MS<sup>3,4</sup>; Anjan Nan, PhD<sup>3,4</sup>; and Hamidreza Ghandehari, PhD<sup>2-4</sup>

<sup>1</sup>Division of Nuclear Medicine, Department of Radiology, University of Maryland School of Medicine, Baltimore, Maryland;

<sup>2</sup>Greenebaum Cancer Center, University of Maryland School of Medicine, Baltimore, Maryland; <sup>3</sup>Center for Nanomedicine

and Cellular Delivery, University of Maryland School of Pharmacy, Baltimore, Maryland; and <sup>4</sup>Department

of Pharmaceutical Sciences, University of Maryland School of Pharmacy, Baltimore, Maryland

Endothelial cells in tumor angiogenesis are highly accessible, genetically stable and present unique molecular markers for targeted therapy. Neoplasia is also characterized by enhanced vascular permeability and disordered lymphatics so that both active and passive targeting strategies may play a role in localizing angiogenesis-targeted agents. To investigate the relative importance of these targeting strategies, the tissue biodistribution of both endothelial-specific and nonspecific peptides and their macromolecular peptide-copolymer conjugates were studied in 2 xenograft models of prostate cancer. Tumor-to-normal tissue background ratios (T/B) of these constructs were compared to evaluate the effect of molecular size on blood clearance and nonspecific vascular permeability. **Methods:** Water-soluble *N*-(2-hydroxypropyl)methacrylamide (HPMA) copolymers were synthesized with side chains terminated in a doubly cyclized Arg-Gly-Asp motif KACDCRGDCFCG (RGD4C: active peptide targeting the  $\alpha_v\beta_3$  integrin) and KACDCRGEFCG (RGE4C: nonactive peptide). The bioactivity of the polymer conjugates and free peptides was characterized in vitro by endothelial cell adhesion assay. The <sup>99m</sup>Tc(CO)<sub>3</sub>-labeled compounds were injected into SCID mice bearing DU145 or PC-3 prostate tumor xenografts for scintigraphic imaging and necropsy organ counting. **Results:** HPMA copolymer-RGD4C conjugates showed similar inhibition of cell adhesion as free RGD4C attached to <sup>99m</sup>Tc(CO)<sub>3</sub> chelator *N*- $\omega$ -bis(2-pyridylmethyl)-L-lysine (RGD4C-DPK) and were significantly higher ( $P < 0.05$ ) than RGE4C, HPMA copolymer-RGE4C, and a hydrolyzed HPMA copolymer precursor. Scintigraphic images obtained at 24 h showed specific tumor localization of HPMA copolymer-RGD4C and RGD4C compared with RGE4C conjugates in both prostate tumor models. Twenty-four-hour necropsy data in the DU145 model showed significantly higher ( $P < 0.001$ ) tumor localization for HPMA copolymer-RGD4C ( $4.60 \pm 1.80$  %ID/g [percentage injected dose per gram tissue]) and RGD4C-DPK ( $3.37 \pm 0.32$  %ID/g) compared with HPMA copolymer-RGE4C ( $1.24 \pm 0.15$  %ID/g) and RGE4C-DPK ( $0.32 \pm 0.04$  %ID/g). Similar results were observed in the PC-3 model. Moreover, higher T/B for the polymer conjugates indicated reduced extravasation of the targeted polymeric conjugates in normal tissues. **Conclusion:** Specific molecular targeting of the

$\alpha_v\beta_3$  integrin and nonspecific vascular permeability are both significant in the relative tumor localization of polymeric conjugates of RGD4C. Extravascular leak in nonspecific organs appears to be a major factor in reducing the T/B for the peptide molecules.

**Key Words:** angiogenesis; HPMA copolymers; RGD peptides; targeted delivery; biodistribution

**J Nucl Med 2005; 46:1552-1560**

Angiogenesis has been identified as a target site for therapeutic intervention because of its important role in tumor growth, metastasis, and inflammatory diseases (1,2). One specific endothelial cell-surface marker, the  $\alpha_v\beta_3$  integrin, has been found to be critical for neovascularization and absent in quiescent blood vessels (3). High-affinity  $\alpha_v\beta_3$ -selective ligands containing the tripeptide sequence Arg-Gly-Asp (RGD) have been identified by phage display studies (4). These RGD peptides have been used to deliver doxorubicin (5) and proapoptotic peptides (6) to the tumor vasculature in targeted chemotherapy. They have also been useful in imaging sites of tumor angiogenesis (7) and may provide a means to deliver molecularly guided radiotherapy to the vascular bed of tumors. Given the role of angiogenesis in the growth and metastasis of tumors, it is important to understand the factors that enhance relative localization at sites of angiogenesis—that is, the ratio of tumor uptake to normal tissue background (T/B).

High T/B is likely to be caused by specific  $\alpha_v\beta_3$  integrin targeting, nonspecific leak through hyperpermeable tumor vessels; rapid clearance of nonlocalized tracer through the kidneys; and restriction of nontargeted agent to the intravascular space in normal vessels. Endothelial integrin targets are immediately accessible to intravascular molecules, so extravascular background activity can be avoided, provided the tracer remains within the blood. To restrict the radiopharmaceuticals to the intravascular space, we have constructed <sup>99m</sup>Tc-labeled conjugates of  $\alpha_v\beta_3$ -targeting peptides and the hydrophilic *N*-(2-hydroxypropyl)methacrylamide (HPMA) copolymer (7,8).

Received Mar. 15, 2005; revision accepted May 12, 2005.

For correspondence or reprints contact: Bruce R. Line, MD, Division of Nuclear Medicine, Department of Radiology, University of Maryland School of Medicine, 22 S. Greene St., Baltimore, MD 21201.

E-mail: bline@umm.edu

The macromolecular copolymer-peptide construct may benefit from a second passive targeting effect. It has long been recognized that macromolecular agents tend to passively accumulate in solid tumors because of high vascular density in tumors, increased permeability and defective architecture of tumor vessels, as well as suppressed lymphatic drainage from the tumor interstitium (9). This phenomenon is known as the enhanced permeability and retention (EPR) effect.

The goal of this project was to evaluate the relative importance of specific targeting and nonspecific vascular permeability in both tumor and normal tissues to understand the factors important in the design of angiogenesis-targeting radiopharmaceuticals. To this end, we compared the biodistribution of  $\alpha_v\beta_3$  integrin-targeting KACDCRGDCFCG peptide (RGD4C) and its control peptide KACDCRGECFCG (RGE4C) to their respective copolymer-peptide conjugates. Studies were performed in SCID mouse human prostate tumor xenograft models using 2 different tumor cell lines (PC-3 and DU145).

## MATERIALS AND METHODS

### Chemicals

RGD4C (KACDCRGDCFCG, molecular weight [MW] 1,273.9) was obtained from AnaSpec Inc. and RGE4C (KACDCRGECFCG, MW 1,288.3) was obtained from Biopolymer Core Facility (University of Maryland, Baltimore, MD). *N*- $\alpha$ -(9-Fluorenylmethoxycarbonyl)-*N*- $\omega$ -bis(2-pyridylmethyl)-L-lysine [(Fmoc) DPK] was a gift from Molecular Insight Pharmaceuticals. Isolink carbonyl reaction kit was a gift from Mallinckrodt Inc. Sodium pertechnetate was obtained from the radiopharmacy at the University of Maryland (Baltimore, MD) from a freshly eluted clinical generator (Mallinckrodt Inc.). *N*-Hydroxysuccinimide (NHS) and dicyclohexylcarbodiimide (DCC) were obtained from Aldrich Chemical Co. All amino acids used were of L-configuration. All other chemicals were of reagent grade and were obtained from Sigma Chemical Co.

### Cell Lines

DU145 human prostate carcinoma cells (American Type Culture Collection) were cultured in Dulbecco's modified Eagle medium (DMEM; Life Technologies Inc.) supplemented with 2 mmol/L L-glutamine, 10% (v/v) heated-inactivated fetal bovine serum (FBS), 1 mmol/L sodium pyruvate, 1.5 g/mL sodium bicarbonate, and 1:100 penicillin/streptomycin. PC-3 human prostate adenocarcinoma cells (American Type Culture Collection) were cultured in Ham's F12K medium (Mediatech Inc.) supplemented with 2 mmol/L L-glutamine, 1.5 g/mL sodium bicarbonate, and 10% (v/v) FBS. For all experimental procedures, confluent cells in culture for 24 h without media change were harvested with 0.05% trypsin/0.02% ethylenediaminetetraacetic acid (EDTA) in phosphate-buffered saline (PBS).

Human umbilical vein endothelial cells (HUVECs; Cambrex Biosciences) were cultured in endothelial cell growth media (500 mL of endothelial cell basal media [EBM] supplemented with 10 ng/mL human recombinant epidermal growth factor [hEGF], 1  $\mu$ g/mL hydrocortisone, 12  $\mu$ g/mL bovine brain extract, 25 U/mL heparin, 50  $\mu$ g/mL gentamicin, 50 ng/mL amphotericin B) containing 2% FBS

at 37°C in a humidified atmosphere of 5% CO<sub>2</sub> (v/v). The cells were detached using 0.05% trypsin/0.02% EDTA in PBS.

### Mouse Xenograft Model of Human Prostate Cancer

Detached DU145 or PC-3 cells were collected, washed, counted, and resuspended in RPMI 1640 media. Cells (10<sup>5</sup>) mixed with Matrigel (Becton Dickinson Labware) were xenografted subcutaneously in the left or right front subaxillary zone of each male Harlan C.B-17/IcrHsd SCID mouse (4- to 6-wk old, 25–30 g). Experiments were initiated when the tumors reached a size of 1–1.5 cm in diameter. During experiments the animals were sedated with an intraperitoneal injection of 2.5% avertin (0.02 mL/g body weight) and studied under an approved protocol of the Institutional Animal Care and Use Committee of the University of Maryland, Baltimore.

### Synthesis and Characterization of Comonomers

Comonomers—i.e., *N*-(2-hydroxypropyl)methacrylamide (HPMA) (melting point [m.p.] 66°C–68°C, MW 143.8) (10); reactive ester comonomer, *N*-methacryloylglycylglycyl-*p*-nitrophenyl ester (MA-GG-ONp) ( $\epsilon_{273} = 9,280.7 \text{ mol/L}^{-1}\cdot\text{cm}^{-1}$ , m.p. 160°C–163°C, MW 321.7) (11); <sup>99m</sup>Tc(CO)<sub>3</sub>-chelating comonomer, *N*-methacryloylglycylglycyl-(*N*- $\omega$ -bis(2-pyridylmethyl)-L-lysine) (MA-GG-DPK) ( $\epsilon_{260} = 5,662.3 \text{ mol/L}^{-1}\cdot\text{cm}^{-1}$ , MW 510.1) (8); and iodine-coupling comonomer, *N*-methacryloyltyrosinamide (MA-Tyr) (m.p. 194°C–196°C, MW 248.2) (12)—were synthesized and characterized according to previously described methods.

### Synthesis and Characterization of HPMA Copolymer-Peptide Conjugates

HPMA copolymers were synthesized by free radical precipitation copolymerization of comonomers in 4% (v/v) dimethyl sulfoxide in acetone using *N,N'*-azobisisobutyronitrile as the initiator (10). The feed composition of the comonomers was kept at 20 mol% for MA-GG-ONp, 5 mol% for MA-GG-DPK, 2 mol% for MA-Tyr, and 73 mol% for HPMA. The comonomer mixtures were sealed in an ampule under nitrogen and stirred at 50°C for 24 h. The precipitated copolymeric precursor was dissolved in methanol and reprecipitated in acetone:ether (3:1) to obtain the pure product. The contents of MA-GG-DPK and MA-Tyr in the copolymers were determined by amino acid analysis (Commonwealth Biotechnologies). MA-GG-ONp content was assessed by release of ONp from the polymer in 1.0N sodium hydroxide by ultraviolet (UV) spectrophotometry (400 nm). Weight average molecular weight ( $M_w$ ) and molecular weight distribution (polydispersity, calculated as weight average molecular weight/number average molecular weight) were estimated by size-exclusion chromatography (SEC) on a Superose 12 column (10 mm  $\times$  30 cm) (Amersham Biosciences) using a fast-protein liquid chromatography system (Amersham Biosciences).

As previously described (7), the HPMA copolymer-peptide conjugates (Fig. 1) were synthesized via *p*-nitrophenyl ester aminolysis of the polymeric precursor, coupling either RGD4C (active peptide) or RGE4C (control peptide with no affinity toward  $\alpha_v\beta_3$ ). RGD4C or RGE4C was dissolved in dry *N,N*-dimethylformamide (DMF), dried over 4-Å molecular sieves. With constant stirring, polymeric precursor in dry DMF and dry pyridine (1:1 molar equivalents relative to the polymeric ONp content) were added to the peptide solution (1.3 times excess molar equivalents relative to ONp). The reaction mixture was bubbled with nitrogen and continuously stirred at room temperature for 22 h. The reaction was terminated with 84  $\mu$ L of 0.1N sodium hydroxide. The crude conjugates were dialyzed against deionized water and lyophilized.

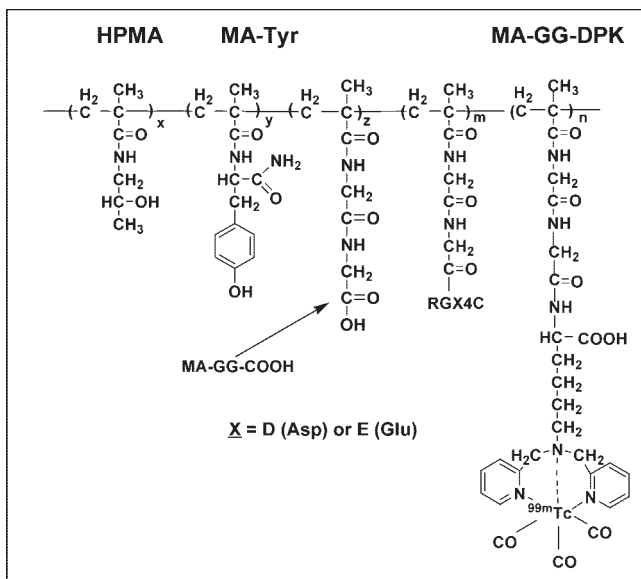


**FIGURE 1.** HPMA copolymer-peptide conjugates labeled with  $^{99m}\text{Tc}(\text{CO})_3$ . Side-chain terminating in *N*- $\omega$ -bis(2-pyridylmethyl)-L-lysine (DPK) was used to label conjugate with  $^{99m}\text{Tc}(\text{CO})_3$ . Conjugate was rendered a negative charge by exposing carboxyl groups of methacryloyl-glycylglycine comonomer residue (MA-GG-COOH) by hydrolysis of *p*-nitrophenyl ester in side chain.

The peptide content in the conjugates was analyzed by amino acid analysis. Conjugate molecular weight was determined by SEC.

### Synthesis and Characterization of Peptide-DPK Conjugates

To prepare RGD4C-DPK and RGE4C-DPK conjugates (Fig. 2), a *N*-hydroxysuccinimidyl ester of (Fmoc) DPK [(Fmoc) DPK-

NHS] was first synthesized (13). Briefly, NHS was added at 2:1 molar excess to (Fmoc) DPK in dry DMF at room temperature. The reaction mixture was then cooled to 0°C, and DCC (molar equivalent to NHS) in dry DMF was added dropwise under constant stirring. The reaction mixture was stirred for 48 h at 4°C. Thereafter, acetic acid (150  $\mu\text{L}$ ) was added and stirred for an additional 1 h. The precipitated dicyclohexylurea was filtered off and the filtrate was concentrated under vacuum. The (Fmoc) DPK-NHS was precipitated in ether, crystallized from isopropanol, and characterized using mass spectrometry (MW 647.3). Next, a 5:1 molar ratio of (Fmoc) DPK-NHS was added to RGD4C or RGE4C in dry DMF and the solution was stirred at room temperature for 24 h. The DMF was evaporated under vacuum, and product formation was confirmed by mass spectrometry [RGD4C-DPK (Fmoc) 1,805.2 and RGE4C-DPK (Fmoc) 1,820.3]. Finally, the Fmoc protection was removed by dissolving the crude product precipitate in 20% piperidine/DMF and stirring at room temperature for 10 min. After vacuum evaporation of residual solvent, the precipitate was washed with 2:1 ether:chloroform, reconstituted in water, and loaded on a C18 Sep-Pak Plus cartridge (Waters Corp.) preconditioned with 5 mL methanol followed by 5 mL water. The loaded cartridge was washed with 5 mL water and the peptide conjugate was eluted with 50% methanol/water. The fractions with highest concentrations of conjugates (as determined by mass spectrometry) were pooled and lyophilized. The peptide conjugates (RGD4C-DPK or RGE4C-DPK) were characterized by mass spectrometry and amino acid analysis.

### $^{99m}\text{Tc}$ -Tricarbonyl Radiolabeling of Conjugates

The conjugates were radiolabeled via  $^{99m}\text{Tc}$ -tricarbonyl coupling to DPK (Figs. 1 and 2) (8). First,  $^{99m}\text{Tc}$ -tricarbonyl [ $^{99m}\text{Tc}(\text{H}_2\text{O})_3(\text{CO})_3$ ] was formed by boiling 1 mL of sodium pertechnetate ( $\text{NaTcO}_4$ ) with sodium tartarate, sodium borate, sodium carbonate, and sodium boranocarbonate (Isolink carbonyl reaction kit; Mallinckrodt Inc.) for 20 min. Second, 120  $\mu\text{L}$  of 1N hydro-

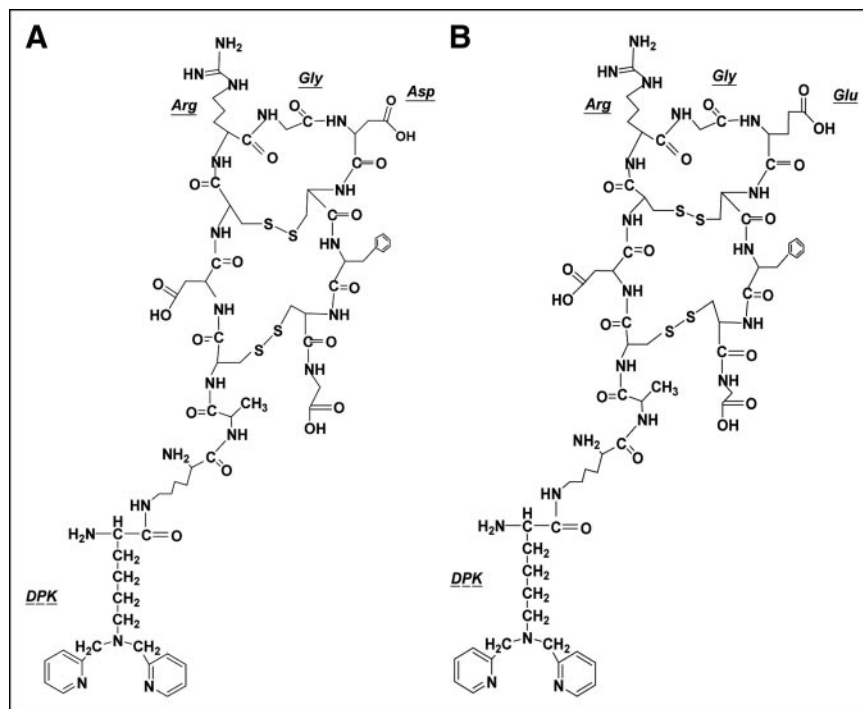


**FIGURE 2.** (A) RGD4C-DPK (KACDCRG-DCFCG), doubly cyclized  $\alpha_v\beta_3$  active peptide with 2 disulfide linkages containing a conformationally restrained RGD site. (B) RGE4C-DPK (KACDCRGEFCG), control peptide with no affinity for  $\alpha_v\beta_3$  integrins. Peptides were conjugated with *N*- $\omega$ -bis(2-pyridylmethyl)-L-lysine (DPK), which was used to label peptides with  $^{99m}\text{Tc}(\text{CO})_3$ .

chloric acid was added to the kit vial to neutralize the solution (pH ~ 6–7) and decompose any residual boranocarbonate. Five hundred microliters of the conjugate solution in normal saline were added to the reaction vial and heated for 30 min at 75°C. The labeled conjugates were purified over a Sephadex G-25 column (PD-10 desalting column; Amersham Biosciences) using normal saline.

The radiochemical purity of the  $^{99m}\text{Tc}(\text{CO})_3$ -labeled peptide-DPK conjugates was determined using instant thin-layer chromatography (ITLC-SG plates; Pal Corp.) with normal saline and 2-butanone as the developing solvent.

### Endothelial Cell Adhesion Assay

The bioactivity of the peptides and copolymer-peptide conjugates was assessed using a HUVEC adhesion assay (14). Flat-bottom 96-well culture plates (Corning Inc.) were coated with 0.5  $\mu\text{g}/\text{well}$  fibrinogen overnight at 4°C. After 3 rinses with PBS, the wells were blocked with 3% bovine serum albumin (BSA) for 1 h at 37°C and washed 3 times with PBS. Trypsinized HUVECs were resuspended in serum-free media and incubated in separate experiments with (a) HPMA copolymer-RGD4C conjugates (HPMA-RGD4C), (b)  $^{99m}\text{Tc}$ -HPMA-RGD4C, (c) HPMA copolymer-RGE4C conjugates (HPMA-RGE4C), (d) ONp hydrolyzed HPMA copolymer precursor (HPMA), (e) RGD4C-DPK, (f) RGE4C-DPK, (g) RGD4C, and (h) RGE4C for 15 min at 22°C. The treated HUVECs were plated at  $3 \times 10^4$  cells per well and allowed to attach for 1 h at 37°C. After incubation the unattached cells were removed by rinsing the wells with PBS. The attached cells were fixed with 3.7% formaldehyde and stained with 0.5% crystal violet. Wells containing 0.1 mol/L citric acid were assayed at 540 nm on a microplate reader (SpectraMax Plus; Molecular Devices). Nonspecific binding was determined by adhesion on BSA-coated plates. All adhesion studies were performed in triplicate. One-way ANOVA was used to test the significance of the differences between compounds in inhibiting HUVEC adhesion.

### Imaging and Biodistribution Studies

Anesthetized animals were injected via the lateral tail vein with 200  $\mu\text{L}$  of normal saline containing 31.2–34.9 nmol of  $^{99m}\text{Tc}(\text{CO})_3$ -labeled HPMA-RGD4C, HPMA-RGE4C, and HPMA (14.8–18.5 MBq) as well as peptide molar equivalents of RGD4C-

DPK and RGE4C-DPK. To assess the early organ biodistribution, sequential 5-min images were obtained for 75 min immediately after intravenous injection using a DSX-LI dual-head  $\gamma$ -camera with a low-energy, all-purpose collimator (SMV America).

At 24 h, a 30-min scintigraphic image was obtained to evaluate residual organ activity. At the time of euthanasia, blood samples were collected by cardiac puncture. During necropsy, whole organ tissue samples were obtained from the heart, lung, liver, spleen, kidney, muscle, and tumor. The tissue samples were washed with water, counted (Cobra II Autogamma; Packard Instruments), and weighed and the percentage injected dose per gram tissue (%ID/g) was calculated. All biodistribution studies were performed with 6 mice per group. To test the significance of the differences in organ accumulation between the compounds, a 1-way ANOVA was used.

## RESULTS

The molecular weight, molecular weight distribution (polydispersity), and side-chain contents of the copolymer precursor and the copolymer-peptide conjugates are shown in Table 1. The side-chain contents in the copolymer precursor were consistent with their corresponding feed comonomer compositions during copolymerization. The contents of MA-GG-DPK and MA-Tyr in the copolymers were 0.2021 and 0.0914 mmol/g, corresponding to 80.8% and 90.6% feed comonomer contents, respectively. The copolymers contained approximately 6 DPK and 3 Tyr units per polymer backbone. The percentage conversions of *p*-nitrophenyl ester (ONp) in the polymeric precursor to RGD4C and RGE4C in the conjugates were 63% and 64.9%, respectively. The conjugates contained about 15 RGD4C and 16 RGE4C moieties per polymer backbone, as determined from amino acid analysis and SEC. The SEC profiles also indicated the absence of free peptides in the polymeric conjugates. The molecular weights were determined to be 1,583.1 for RGD4C-DPK and 1,598.5 for RGE4C-DPK. Amino acid analyses also confirmed the successful synthesis of RGD4C-DPK and RGE4C-DPK.

**TABLE 1**  
Physiochemical Characteristics of HPMA Copolymer Precursor, HPMA Copolymer-RGD4C Conjugate, and HPMA Copolymer-RGE4C Conjugate

| Characteristic                                 | HPMA copolymer precursor | HPMA-RGD4C conjugate | HPMA-RGE4C conjugate |
|--|--------------------------|----------------------|----------------------|
| Estimated $M_w$ (kDa)*                         | 28.6                     | 30.2                 | 32.4                 |
| Polydispersity*                                | 1.3                      | 1.5                  | 1.6                  |
| ONp content (mmol/g polymer) <sup>†</sup>      | 0.783 $\pm$ 0.011        | —                    | —                    |
| DPK content (mmol/g polymer) <sup>‡</sup>      | 0.2021 (6)               | —                    | —                    |
| Tyr content (mmol/g polymer) <sup>‡</sup>      | 0.0914 (3)               | —                    | —                    |
| RGD4C or RGE4C (mmol/g polymer) <sup>‡</sup>   | —                        | 0.4936 (15)          | 0.5089 (16)          |
| Carboxyl content (mmol/g polymer) <sup>§</sup> | —                        | 0.2894 (9)           | 0.2741 (8)           |

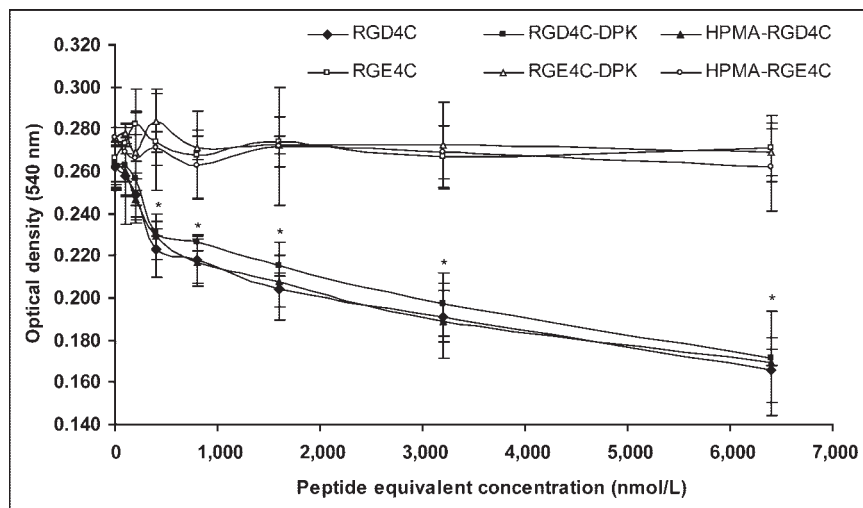
\*As determined by SEC.

<sup>†</sup>Results of UV spectrophotometric analysis. Values represent mean  $\pm$  SD ( $n = 3$ ).

<sup>‡</sup>Results of amino acid analysis (numbers in parentheses represent approximate number of groups per polymer).

<sup>§</sup>Results of subtraction between ONp content and RGD4C or RGE4C content.

**FIGURE 3.**  $\alpha_v\beta_3$ -mediated adhesion of HUVECs to fibrinogen was inhibited on exposure of HUVECs to HPMA copolymer-RGD4C conjugate, RGD4C-DPK, and free RGD4C (solid symbols, lower curves). Controls—namely, HPMA copolymer-RGE4C conjugate, RGE4C-DPK, and free RGE4C (open symbols, upper curves)—showed no inhibition of adhesion. Values represent means of triplicates  $\pm$  SD (\* $P < 0.05$  compared with controls).



$^{99m}\text{Tc}(\text{CO})_3$  radiolabeling of the copolymer conjugates achieved efficiencies of  $>93\%$ , with specific activities of 16.8–19.5 MBq/nmol. Similarly, radiolabeling of the peptide-DPK conjugates yielded radiolabeling efficiencies of  $>95\%$ . After purification, the radiochemical purity was  $>98.9\%$ , with specific activities of  $>8.3$  MBq/nmol.

The endothelial cell adhesion assay results are summarized in Figure 3. HPMA copolymer-RGD4C conjugates (HPMA-RGD4C), RGD4C-DPK, and free RGD4C caused similar degrees of inhibition of endothelial cell adhesion to fibrinogen at equivalent molar concentrations of RGD4C. In contrast, HPMA copolymer-RGE4C conjugate (HPMA-RGE4C), RGE4C-DPK, and free RGE4C showed no inhibition of cell adhesion. Similarly, the ONp-hydrolyzed HPMA copolymer precursor (HPMA) showed no inhibition (data not shown). Above 400 nmol/L equivalent peptide concentrations, RGD4C-containing conjugates showed significantly higher ( $P < 0.05$ ) inhibition of cell adhesion than that of RGE4C conjugates. Radiolabeling of the RGD4C peptides or HPMA-RGD4C conjugates with  $^{99m}\text{Tc}(\text{CO})_3$  did not alter inhibition of cell adhesion (data not shown).

Scintigraphic images of SCID mice bearing prostate tumor xenografts 24 h after injection are shown in Figure 4. The HPMA-RGD4C conjugates clearly showed higher tumor localization in both xenograft models (DU145 and PC-3) compared with HPMA-RGE4C conjugates. Similarly, RGD4C-DPK showed significantly higher tumor accumulation relative to RGE4C-DPK.

The 24-h necropsy radioactivity was expressed as %ID/g. In the DU145 xenograft model (Fig. 5), HPMA-RGD4C ( $4.60 \pm 1.80$  %ID/g) and RGD4C-DPK ( $3.37 \pm 0.32$  %ID/g) showed significantly higher tumor accumulation ( $P < 0.001$ ) than HPMA-RGE4C ( $1.24 \pm 0.15$  %ID/g), RGE4C-DPK ( $0.32 \pm 0.04$  %ID/g), or HPMA ( $1.26 \pm 0.11$  %ID/g). The blood activity of HPMA-RGD4C ( $0.255 \pm 0.06$  %ID/g) was higher ( $P < 0.001$ ) than RGD4C-DPK ( $0.111 \pm 0.01$  %ID/g), suggesting longer circulation times for the polymeric conjugates. RGD4C-DPK showed significantly higher ( $P < 0.001$ ) organ (heart, lung, liver, spleen, and kidney) activity compared with HPMA-RGD4C, suggesting greater nonspecific extravascular distribution (“leak”). HPMA-RGD4C also had a significantly higher

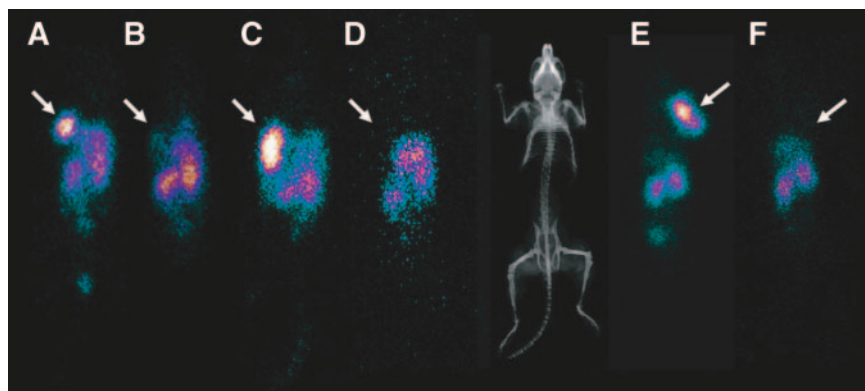


**FIGURE 4.** Scintigraphic images of SCID mice bearing prostate tumor xenografts 24 h after intravenous injection of  $^{99m}\text{Tc}(\text{CO})_3$ -labeled conjugates. Intravenously injected HPMA copolymer-RGD4C conjugate (A and E) and RGD4C-DPK (C) showed marked localization in tumor as compared with HPMA copolymer-RGE4C conjugate (B and F) and RGE4C-DPK (D). Free peptides (RGD4C-DPK and RGE4C-DPK) also showed higher background accumulation in liver, spleen, and abdominal regions. Arrows mark location of tumor. Mouse radiograph shows anatomic correlation of tumor and other organs. (A–D) SCID mice with DU145 tumor xenografts. (E and F) Mice with PC-3 tumor xenografts.

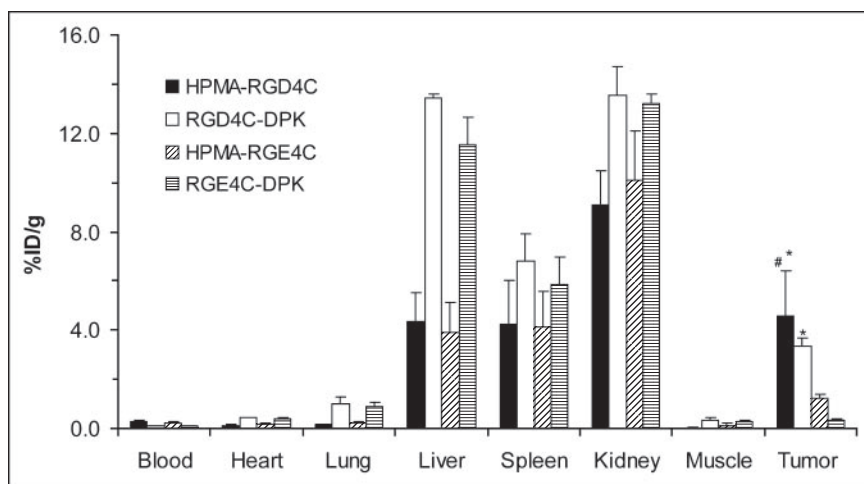


**FIGURE 5.** Residual radioactivity in %ID/g of organ tissue 24 h after intravenous injection of  $^{99m}\text{Tc}(\text{CO})_3$ -labeled copolymer conjugates and peptides in DU145 prostate tumor xenograft-bearing SCID mice. Organ data are expressed as mean  $\pm$  SD (number of animals/group is shown). \* $P < 0.001$  compared with HPMA copolymer-RGE4C conjugate and RGE4C-DPK. # $P < 0.05$  compared with RGD4C-DPK.

( $P < 0.05$ ) tumor accumulation than RGD4C-DPK. The tumor/organ background ratios for all the normal organs except blood (Table 2) were significantly higher ( $P < 0.001$ ) for the polymer conjugates (HPMA-RGD4C and HPMA-RGE4C) than their corresponding free peptides (RGD4C-DPK and RGE4C-DPK). Furthermore, HPMA-RGD4C showed significantly higher ( $P < 0.001$ ) tumor/organ background ratios relative to RGD4C-DPK, HPMA-RGE4C, and RGE4C-DPK.

Similar results were obtained for the PC-3 xenograft model (Fig. 6). The tumor uptake of HPMA-RGD4C ( $5.92 \pm 0.41$  %ID/g) and RGD4C-DPK ( $4.41 \pm 0.23$  %ID/g) was higher ( $P < 0.001$ ) than HPMA-RGE4C ( $1.28 \pm 0.06$  %ID/g) and RGE4C-DPK ( $0.34 \pm 0.07$  %ID/g). The tumor accumulation of HPMA-RGD4C was significantly higher ( $P < 0.001$ ) than RGD4C-DPK. The blood activity of HPMA-RGD4C ( $0.323 \pm 0.03$  %ID/g) was higher ( $P < 0.001$ ) than RGD4C-DPK ( $0.123 \pm 0.01$  %ID/g). Again, the uptake of RGD4C-DPK was higher than HPMA-RGD4C ( $P < 0.001$ ) in all organs (heart, lung, liver, spleen, and kidney). As with the DU145 tumor, the tumor/organ background ratios (Table 2) were higher ( $P < 0.001$ ) for the polymer conjugates than the peptides and highest for HPMA-RGD4C.

## DISCUSSION

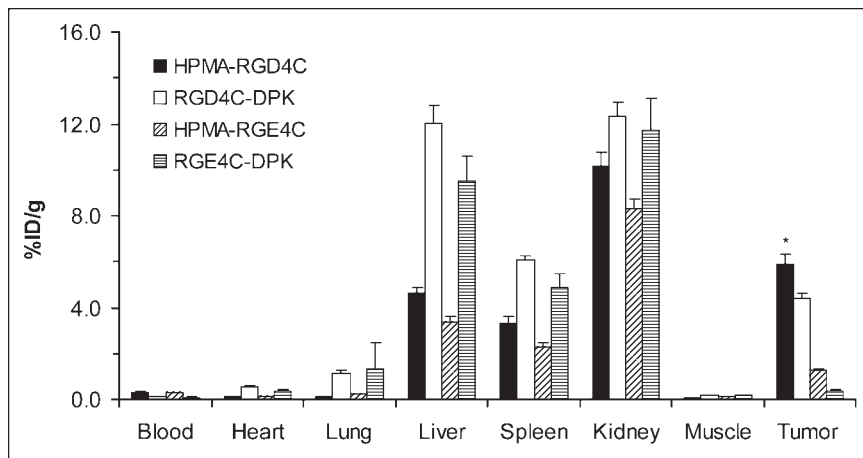
Angiogenesis is the process by which new capillaries sprout from existing vessels to support tumor growth and metastasis (1,2,15). Without adequate vasculature, tumor cells become necrotic or apoptotic (3,16). The relationship between angiogenesis and tumor progression is well established. As summarized by Weidner (15), microvascular density is found to have independent prognostic significance when compared with traditional prognostic markers by multivariate analysis in a wide variety of cancers, including malignant melanomas, multiple myeloma, central nervous system tumors, and carcinomas of the breast, prostate, lung, head and neck, nasopharynx, gastrointestinal tract, bladder, endometrium, ovaries, testes, and reproductive tract.

Of the molecular markers associated with neovascular angiogenesis,  $\alpha_v\beta_3$  integrin, an endothelial cell-surface receptor of vitronectin, is concentrated on the apical surface of forming blood vessels and is absent or barely detectable in established blood vessels (3,17,18). Thus, the early appearance of an angiogenic response in a tumor (relative to tumor growth), the highly selective expression of  $\alpha_v\beta_3$  integrins in the neovascular tissue in a broad spectrum of tumors, and the critical role the angiogenic response plays in tumor

**TABLE 2**  
Effect of Polymer Conjugation on Mean T/B for  $\alpha_v\beta_3$  Active RGD4C Peptide and Control RGE4C Peptide

| Biodistribution | DU145      |           |            |           | PC-3       |           |            |           |
|-----------------|------------|-----------|------------|-----------|------------|-----------|------------|-----------|
|                 | HPMA-RGD4C | RGD4C-DPK | HPMA-RGE4C | RGE4C-DPK | HPMA-RGD4C | RGD4C-DPK | HPMA-RGE4C | RGE4C-DPK |
| Blood           | 18.03      | 30.28     | 5.46       | 3.25      | 18.29      | 35.94     | 4.36       | 3.99      |
| Heart           | 37.10      | 7.62      | 7.82       | 0.81      | 43.80      | 8.41      | 9.32       | 0.99      |
| Lung            | 29.97      | 3.28      | 5.98       | 0.35      | 40.56      | 3.84      | 5.94       | 0.26      |
| Liver           | 1.05       | 0.25      | 0.32       | 0.03      | 1.29       | 0.37      | 0.38       | 0.04      |
| Spleen          | 1.08       | 0.49      | 0.30       | 0.05      | 1.80       | 0.73      | 0.56       | 0.07      |
| Kidney          | 0.51       | 0.25      | 0.12       | 0.02      | 0.58       | 0.36      | 0.15       | 0.03      |
| Muscle          | 166.62     | 10.64     | 9.00       | 1.15      | 89.63      | 22.43     | 12.81      | 1.89      |

**FIGURE 6.** Residual radioactivity in %ID/g of organ tissue 24 h after intravenous injection of  $^{99m}\text{Tc}(\text{CO})_3$ -labeled copolymer conjugates and peptides in PC-3 prostate tumor xenograft-bearing SCID mice. Organ data are expressed as mean  $\pm$  SD (number of animals/group is shown). \* $P < 0.001$  compared with HPMA copolymer-RGE4C conjugate, RGD4C-DPK, and RGE4C-DPK.



growth and progression make this an excellent target for both diagnostic imaging and directed therapy (1,2,18).

The RGD peptide (RGD4C, Fig. 2) used in this study has a conformationally restrained RGD sequence because of the presence of 2 disulfide bridges and binds specifically and with high affinity to  $\alpha_v\beta_3$  (19). The control peptide (RGE4C, Fig. 2) had identical structure, length, and sequence as that of RGD4C with the only exception of a glutamic acid residue in RGE4C instead of an aspartic acid residue, a single carbon difference.

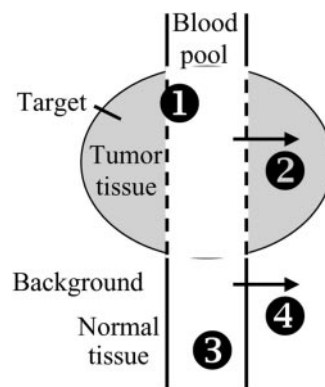
The bioactivity of the peptides and copolymer-peptide conjugates was evaluated by inhibition of endothelial cell (HUVEC) adhesion on fibrinogen-coated surfaces. Endothelial cell-surface integrins such as  $\alpha_v\beta_3$  adhere to matrix proteins via binding to fibrinogen and vitronectin (14). This attachment is competitively inhibited by RGD-containing peptides. HPMA-RGD4C, RGD4C-DPK, and native RGD4C showed similar levels of inhibition of HUVEC adhesion when used with equimolar amounts of RGD4C. Because the inhibition was only caused by the RGD4C conjugates and not by RGE4C conjugates or the HPMA copolymer, it is reasonable to conclude that the RGD4C conjugates bind to the endothelial cell surface via the RGD motif. Labeling of the conjugates with  $^{99m}\text{Tc}(\text{CO})_3$  did not reduce the adhesion inhibition, suggesting that the heating steps and labeling agents did not substantially change the bioactivity.

Figure 7 shows our conceptual model of the main compartments and factors that should influence the T/B in the vicinity of a tumor. Factors expected to increase the signal from T, the angiogenesis target, include (1) specific uptake at endothelial site (i.e., RGD4C binding to  $\alpha_v\beta_3$ ), and (2) tumor EPR or binding in the tumor. Tumor binding may be nonspecific or may be due to specific coupling when  $\alpha_v\beta_3$  integrin is expressed by tumor cells (20). Factors increasing B, the background, include (3) persistence of activity in the blood pool and (4) extravascular leak or nonspecific binding in normal tissues. Tracer elimination from the body can reduce both body background and the buildup of target activity but, for the purposes of this conceptual model, the

activity lost from the system is not relevant to the T/B at the time of imaging.

Radiolabeled RGD4C was expected to provide good-to-excellent T/B at sites of tumor angiogenesis given the highly selective expression of  $\alpha_v$  integrins in the neovascular tissue of the tumor (high 1). Specific localization of the RGD peptide and copolymer-peptide was verified by significantly higher tumor uptake relative to RGE compounds in both tumor models. Both the necropsy data and the scintigraphic images obtained at 24 h after injection were clearly different for the RGD and RGE free peptides. Similarly, the increased tumor intensity for the HPMA-RGD4C conjugates relative to the HPMA-RGE4C conjugates was most likely due to the interaction of the  $\alpha_v\beta_3$  integrin with the RGD motifs on the conjugates.

There was significantly higher tumor uptake of HPMA-RGD4C conjugate relative to RGD4C and there was significantly higher tumor uptake of HPMA-RGE4C conjugate



**FIGURE 7.** Conceptual model of factors influencing tumor-to-normal tissue background ratios (T/B) in vicinity of a tumor. Factors that increase detection signal from tumor target include (1) specific uptake at a molecular targeting site (i.e., binding to  $\alpha_v\beta_3$ ) and (2) vascular leak within tumor bed or nonspecific binding in tumor. Factors that decrease T/B are largely due to background activity sources, including (3) persistence of activity in blood pool and (4) extravascular leak or nonspecific binding in normal tissues.

relative to RGE4C. The similar difference between the copolymer-peptide and peptide for both RGD and RGE in both tumor models suggests that this difference was likely related to EPR (2) of the macromolecules. EPR is, in part, related to changes that occur during angiogenesis. To stimulate angiogenesis, tumors secrete an endothelial cell-specific mitogen, vascular endothelial growth factor (VEGF), which significantly increases vascular permeability to macromolecules (21–23). Plasma proteins extravasate from leaky tumor blood vessels and form a new extravascular matrix that favors the migration of endothelial cells and fibroblasts (24–26). Direct measurements with macromolecular tracers have clearly demonstrated hyperpermeability of the microvessels supplying tumors (21,26,27). In contrast, the agents are not detected outside the vasculature of normal skin, subcutaneous tissue, and skeletal muscle (28,29). However, the higher tumor accumulation of HPMA-RGD4C conjugate relative to RGD4C could also be due to multivalency of the targeting moiety on the polymer backbone. For example, dimeric  $^{99m}\text{Tc}$ -HYNIC-E-[c(RGDfK)]<sub>2</sub> peptide has a 10-fold higher affinity than that of the  $^{99m}\text{Tc}$ -HYNIC-c(RGDfK) monomer as well as significantly higher renal retention (30). Dimeric and tetrameric complexes of c(RGDfK) have been labeled with  $^{18}\text{F}$ , the dimeric form showing enhanced tumor binding relative to  $^{18}\text{F}$ -Galacto-RGD (31).

The early scintigraphic images (0–1 h) showed more rapid clearance of the peptide activity from the cardiac blood-pool region in comparison with the copolymer-peptide conjugates (6) but, at 24 h, although the difference was statistically significant, the blood pool was a minor contributor to the body biodistribution (Figs. 5 and 6).

The interstitial diffusion coefficient and microvascular permeability of small molecules (MW <2,000) is almost equal in normal and neoplastic tissues (32). The T/B for peptide tracers would therefore not be expected to benefit from the EPR effect. The  $\alpha_v\beta_3$  target is immediately accessible to the intravascular space, so targeted tracers do not need to diffuse into the extravascular space like other tumor-targeting agents. For the same reason, background activity from normal extravascular tissue can be avoided, provided the  $\alpha_v\beta_3$ -targeting tracer remains within the blood. The incorporation of slight negative charge (Table 1) on the hydrophilic HPMA copolymer conjugate helps to restrict extravascular migration of the tracer in normal vascular beds. The amount of extravascular migration and retention of the tracers (4) was clearly organ related but, at 24 h, there was a significantly higher activity for the free peptides, relative to the copolymer-peptide conjugates, for all organs analyzed (heart, lung, liver, spleen, kidney, muscle).

For all the agents tested, the combination of HPMA copolymer and the RGD4C peptide was found to provide the highest contrast of cancer xenografts relative to normal tissues (Table 2). High T/B is likely to be due to specific  $\alpha_v\beta_3$  targeting (high 1); leak of HPMA-RGD4C through tumor vessels (high 2); clearance of nonlocalized HPMA-

peptide conjugates through the kidneys (low 3); and restriction of HPMA conjugates to the intravascular space in normal vessels (low 4).

It is interesting that the nonspecific copolymer-peptide conjugate, HPMA-RGE4C conjugate showed a similar or higher tumor to organ ratio relative to the specifically targeted RGD4C peptide. Although HPMA-RGE4C conjugate had low absolute tumor localization, the explanation for this nonintuitive result is likely due to the relatively high extravascular leak of RGD4C in normal tissues (4). The other T/B relationships in Table 2 are likely due to the fact that RGD4C does not benefit from EPR to the same extent as HPMA-RGE4C conjugate and RGE4C benefits from neither specific targeting nor EPR.

Although the organ activity for the polymer-peptide conjugates was lower than the free peptide, the levels in the liver, spleen, and kidney are comparable with or higher than the tumor uptake. High liver and spleen localization has been noted for  $\alpha_v\beta_3$ -targeting molecules possibly due to their hydrophobic quality or to specific binding. Janssen et al. found that the uptake in the liver, spleen, and lung was much smaller for compounds containing a scrambled control molecule, c(RGKfD), as compared with c(RGDfK) (33). Other modifications, such as increasing copolymer electronegative charge (8,34) or reducing the size of the macromolecule (8,35,36), may help decrease these localizations. In prior studies (8), we evaluated the fate and the total body distribution of  $^{99m}\text{Tc}(\text{CO})_3$ -HPMA copolymers (MW 7, 21, and 70 kDa) in nontumor-bearing SCID mice over 24 h. The renal elimination rate was found to be dependent on molecular weight and electronegative charge, with the charge having the predominant effect on biodistribution. Except for the kidney, at both 90 min and 24 h, the 70-, 21-, and 7-kDa  $^{99m}\text{Tc}(\text{CO})_3$ -HPMA copolymers demonstrated progressively smaller tissue activity. The highest uptake of the neutral 70-kDa fraction was seen in lung, liver, and spleen. The electronegative copolymers did not localize to a significant extent by any body organ other than the kidneys.

Over the past decade,  $\alpha_v\beta_3$ -targeting molecules have been developed with designs to enhance targeting affinity, biodistribution, and renal clearance (7,30,37,38). Sufficiently rapid clearance has been achieved through glycosylation of a cyclized peptidomimetic to be applied in  $^{18}\text{F}$  PET (39,40). Strategies of design may emphasize small molecular weight to enhance renal clearance when very short-lived tracers are used or may seek to exploit ligand multivalency to enhance target affinity when using longer-lived therapeutic isotopes.

The  $\alpha_v\beta_3$  ligand is present not only on the vascular endothelium but is also expressed by some tumor cells, mediating extracellular matrix adhesion and tumor invasion (20,41). Given that there is likely to be little vascular permeability difference between the peptide-polymer conjugates and the peptides in the leaky tumor vessels, it is yet to be determined if there is a substantial peptide advantage in targeting  $\alpha_v\beta_3$  ligands on tumor cells.

## CONCLUSION

Several factors appear to influence the biodistribution of angiogenesis-targeting RGD4C conjugates. Specific targeting of the  $\alpha_v\beta_3$  integrin and nonspecific vascular permeability are both significant, but specific targeting is more important than EPR of the carrier molecule. Nonspecific vascular permeability appears to be a major factor in reducing tumor-to-normal tissue localization ratio for the peptide molecules. These results may have relevance to the design of angiogenesis-targeted complexes for diagnosis and therapy of solid tumors.

## ACKNOWLEDGMENTS

The authors thank John W. Babich (Molecular Insight Pharmaceuticals) for providing DPK; Mary Dyszlewski (Mallinckrodt Inc.) for providing the Isolink carbonyl reaction kit; Kristin Lanham for imaging experiments; and Edwina McNeill for biodistribution experiments and laboratory management. This research was supported by National Institutes of Health grants R21 CA81492-01A1 and R21 CA91770A and by Department of Defense grant DAMD170010004.

## REFERENCES

- Carmeliet P. Angiogenesis in health and disease. *Nat Med*. 2003;9:653–660.
- Folkman J. Tumor angiogenesis: therapeutic implications. *N Engl J Med*. 1971;285:1182–1186.
- Brooks PC, Clark RA, Cheresh DA. Requirement of vascular integrin alpha v beta 3 for angiogenesis. *Science*. 1994;264:569–571.
- Pasqualini R, Koivunen E, Ruoslahti E. Alpha v integrins as receptors for tumor targeting by circulating ligands. *Nat Biotechnol*. 1997;15:542–546.
- Arap W, Pasqualini R, Ruoslahti E. Cancer treatment by targeted drug delivery to tumor vasculature in a mouse model. *Science*. 1998;279:377–380.
- Ellerby HM, Arap W, Ellerby LM, et al. Anti-cancer activity of targeted proapoptotic peptides. *Nat Med*. 1999;5:1032–1038.
- Mitra A, Mulholland J, Nan A, McNeill E, Ghandehari H, Line BR. Targeting tumor angiogenic vasculature using polymer-RGD conjugates. *J Control Release*. 2005;102:191–201.
- Mitra A, Nan A, Ghandehari H, McNeill E, Mulholland J, Line BR. Technetium-99m labeled N-(2-hydroxypropyl)methacrylamide (HPMA) copolymers: synthesis, characterization and in vivo biodistribution. *Pharm Res*. 2004;21:1153–1159.
- Maeda H, Wu J, Sawa T, Matsumura Y, Hori K. Tumor vascular permeability and the EPR effect in macromolecular therapeutics: a review. *J Control Release*. 2000;65:271–284.
- Strohalm J, Kopecek J. Poly N-(2-hydroxypropyl)methacrylamide. 4. Heterogeneous polymerization. *Angew Makromol Chem*. 1978;70:109–118.
- Rejmanova P, Labsky J, Kopecek J. Aminolyses of monomeric and polymeric p-nitrophenyl esters of methacryloylated amino acids. *Makromol Chem*. 1977;178:2159–2168.
- Lee JH, Kopeckova P, Kopecek J, Andrade JD. Surface properties of copolymers of alkyl methacrylates with methoxy (polyethylene oxide) methacrylates and their application as protein-resistant coatings. *Biomaterials*. 1990;11:455–464.
- Winnard P Jr, Chang F, Ruscowski M, Mardirossian G, Hnatowich DJ. Preparation and use of NHS-MAG3 for technetium-99m labeling of DNA. *Nucl Med Biol*. 1997;24:425–432.
- Ruegg C, Yilmaz A, Bieler G, Bamat J, Chaubert P, Lejeune FJ. Evidence for the involvement of endothelial cell integrin alphaVbeta3 in the disruption of the tumor vasculature induced by TNF and IFN-gamma. *Nat Med*. 1998;4:408–414.
- Weidner N. Tumour vascularity as a prognostic factor in cancer patients: the evidence continues to grow. *J Pathol*. 1998;184:119–122.
- Brooks PC, Montgomery AM, Rosenfeld M, et al. Integrin alpha v beta 3 antagonists promote tumor regression by inducing apoptosis of angiogenic blood vessels. *Cell*. 1994;79:1157–1164.
- Eliceiri BP, Cheresh DA. Role of alpha v integrins during angiogenesis. *Cancer J*. 2000;6(suppl 3):S245–S249.
- Ruoslahti E. Specialization of tumour vasculature. *Nat Rev Cancer*. 2002;2:83–90.
- Koivunen E, Wang B, Ruoslahti E. Phage libraries displaying cyclic peptides with different ring sizes: ligand specificities of the RGD-directed integrins. *Biotechnology (N Y)*. 1995;13:265–270.
- Felding-Habermann B. Integrin adhesion receptors in tumor metastasis. *Clin Exp Metastasis*. 2003;20:203–213.
- Jain RK. Tumor angiogenesis and accessibility: role of vascular endothelial growth factor. *Semin Oncol*. 2002;29:3–9.
- Yancopoulos GD, Davis S, Gale NW, Rudge JS, Wiegand SJ, Holash J. Vascular-specific growth factors and blood vessel formation. *Nature*. 2000;407:242–248.
- Yuan F, Chen Y, Dellian M, Safabakhsh N, Ferrara N, Jain RK. Time-dependent vascular regression and permeability changes in established human tumor xenografts induced by an anti-vascular endothelial growth factor/vascular permeability factor antibody. *Proc Natl Acad Sci USA*. 1996;93:14765–14770.
- Denekamp J. Review article: angiogenesis, neovascular proliferation and vascular pathophysiology as targets for cancer therapy. *Br J Radiol*. 1993;66:181–196.
- Hood JD, Cheresh DA. Role of integrins in cell invasion and migration. *Nat Rev Cancer*. 2002;2:91–100.
- Jain RK, Munn LL, Fukumura D. Dissecting tumour pathophysiology using intravital microscopy. *Nat Rev Cancer*. 2002;2:266–276.
- Blumenthal RD, Kashi R, Sharkey RM, Goldenberg DM. Quantitative and qualitative effects of experimental radioimmunotherapy on tumor vascular permeability. *Int J Cancer*. 1995;61:557–566.
- Mehvar R, Reynolds JM, Shepard TL. Disposition of fluorescein-labelled dextran (150 kD) in isolated perfused livers from control and diabetic rats. *Life Sci*. 1991;49:1699–1706.
- Mehvar R, Reynolds JM. Pharmacokinetics of 70-kilodalton fluorescein-dextran in experimental diabetes mellitus. *J Pharmacol Exp Ther*. 1993;264:662–669.
- Janssen M, Oyen WJ, Massuger LF, et al. Comparison of a monomeric and dimeric radiolabeled RGD-peptide for tumor targeting. *Cancer Biother Radiopharm*. 2002;17:641–646.
- Poethko T, Schottelius M, Thumshirn G, et al. Two-step methodology for high-yield routine radiohalogenation of peptides: (18)F-labeled RGD and octeotide analogs. *J Nucl Med*. 2004;45:892–902.
- Netti PA, Berk DA, Swartz MA, Grodzinsky AJ, Jain RK. Role of extracellular matrix assembly in interstitial transport in solid tumors. *Cancer Res*. 2000;60:2497–2503.
- Janssen ML, Oyen WJ, Dijkgraaf I, et al. Tumor targeting with radiolabeled alpha(v)beta(3) integrin binding peptides in a nude mouse model. *Cancer Res*. 2002;62:6146–6151.
- Kissel M, Peschke P, Subr V, et al. Biodistribution of charged poly[N-(2-hydroxypropyl)methacrylamide] in tumor bearing rats. [Abstract]. Proceedings of the 28th International Symposium on Controlled Release of Bioactive Materials; June 23–27, 2001; San Diego, CA: 1346–1347.
- Kissel M, Peschke P, Subr V, et al. Synthetic macromolecular drug carriers: biodistribution of poly[(N-2-hydroxypropyl)methacrylamide] copolymers and their accumulation in solid rat tumors. *PDA J Pharm Sci Technol*. 2001;55:191–201.
- Seymour LW, Miyamoto Y, Maeda H, et al. Influence of molecular weight on passive tumour accumulation of a soluble macromolecular drug carrier. *Eur J Cancer*. 1995;31A:766–770.
- Haubner R, Wester HJ, Reuning U, et al. Radiolabeled alpha,beta<sub>3</sub> integrin antagonists: a new class of tracers for tumor targeting. *J Nucl Med*. 1999;40:1061–1071.
- Haubner R, Kuhnast B, Mang C, et al. [<sup>18</sup>F]Galacto-RGD: synthesis, radiolabeling, metabolic stability, and radiation dose estimates. *Bioconjug Chem*. 2004;15:61–69.
- Haubner R, Wester HJ, Weber WA, et al. Noninvasive imaging of alpha,beta<sub>3</sub> integrin expression using <sup>18</sup>F-labeled RGD-containing glycopeptide and positron emission tomography. *Cancer Res*. 2001;61:1781–1785.
- Haubner R, Weber WA, Beer AJ, et al. Noninvasive visualization of the activated alpha,beta<sub>3</sub> integrin in cancer patients by positron emission tomography and [<sup>18</sup>F]galacto-RGD. *Plos Med*. 2005;2:244–252.
- Ruoslahti E, Giancotti FG. Integrins and tumor cell dissemination. *Cancer Cells*. 1989;1:119–126.